A Series/Parallel Magnetic-less Step-Down Converter based on Piezoelectric Resonators

Wen-Chin Liu
Department of Electrical and Computer Engineering
University of California San Diego
La Jolla, USA
brianliu@eng.ucsd.edu

Patrick P. Mercier
Department of Electrical and Computer Engineering
University of California San Diego
La Jolla, USA
pmercier@ucsd.edu

***Abstract*—This study proposes a series/parallel piezoelectric resonator (SPPR) DC-DC converter that strives to improve performance at larger step-down ratios than what baseline piezo-resonator-based (PR) converters can nominally achieve. In the proposed converter, a series/parallel (SP) switched capacitor (SC) network is integrated into a traditional piezo-resonator-based step-down DC-DC converter to improve the performance of the piezo-based converter while maintaining most of the benefits of the traditional PR converter: zero-voltage switching and soft-charging of the junction capacitor in PRs. By leveraging the pre-step-down property of the SC network, the optimal efficiency point can be shifted below the 2:1 ratio where the baseline PR-based converter is most efficient. Moreover, due to the piezoelectric resonator's inductive operation, the flying capacitor of the SC network can achieve soft charging/discharging over all operation ranges. A SPPR prototype is built with lead zirconate titanate (PZT) PRs to verify the operation of the proposed topology, demonstrating a peak efficiency of 95.27% at a 48V to 10V conversion ratio at 1.5W, and up to a 14.17% efficiency improvement over a baseline PR converter.**

***Index Terms*—component, formatting, style, styling, insert**

I. Introduction

Due to their planar form factor, ease of batch fabrication, and linear scaling properties, piezoelectric devices have garnered significant attention toward the design of small, lightweight, and high-efficiency power converters [1]–[7]. Typically, magnetic components can be shrunk as the operating frequency increases; however, the size reduction is not necessarily linear-related to the increment of frequency, limiting miniaturization possibilities [8]. On the other hand, piezoelectric devices generally linear-scale with their resonant frequencies, and therefore, emerging compact converters with high achievable efficiency and power density are becoming possible.

Among piezoelectric devices, piezoelectric resonators (PRs) are reported to show high power density and high-efficiency [9]–[11]. Fig. 1 shows one such high-efficiency PR-based converters. By operating the PR in the inductive resonating region, zero-voltage switching (ZVS) and soft-charging of the PR's junction capacitance can be achieved, leading to low overall losses.

However, previously reported PR-based step-down DC-DC converters usually achieve their optimal efficiency at a conversion ratio of 2:1, and their performance degrades as

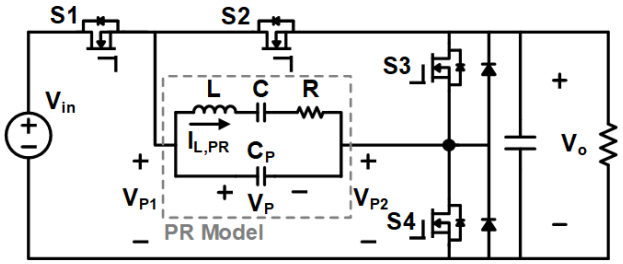

Fig. 1. Baseline step-Down PR-based Converter

conversion deviates from the optimal point [12]. Unfortunately, many step-down converter applications require a much larger conversion ratio, limiting the appeal of a baseline PR-based step-down converter to broad application spaces.

One of the solutions to prevent efficiency degradation in PR-based converter at a higher step-down scenario is to shift the optimal operation point of the converter to the desired conversion ratio. Cascading an additional converter could be an option; however, this leads to cascaded losses and increased component count and control complexity. A better way is to integrate the cascaded converter into the original baseline converter without changing the control law, such as has been popularized by hybrid capacitive/inductive converters.

In this paper, a series/parallel piezoelectric resonator (SPPR) converter is proposed to improve the performance of a PR-based converter when a higher step-down ratio is required. Taking advantage of a pre-step-down SC network integrated into the converter in a similar manner to a hybrid capacitive/inductive converter, the optimal operation point of the entire converter is shifted to a larger step-down ratio while maintaining most of the benefits of traditional PR-based converters. Beneficially, the flying capacitor of the SC network can be soft-charged/discharged due to the inductive operation of the PR, eliminating the charge-sharing loss of the flying capacitor. Here, the proposed topology is mathematically analyzed, simulated in SIMPLIS, and a physical prototype is constructed. Measurement results at a 48/10V conversion ratio with a PZT-based radial mode PR are used to verify the functionality and performance of the proposed topology.

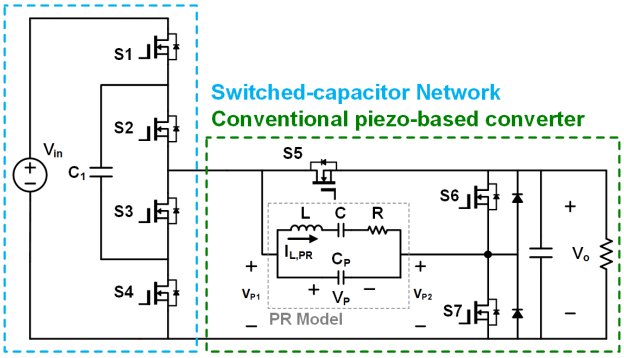

Fig. 2. Circuit diagram of series/parallel piezoelectric resonator converter

II. Proposed Series/Parallel Piezoelectric-Resonator-Based Step-Down Converter

The series/parallel piezoelectric resonator (SPPR) converter is shown in Fig. 2, where the PR is represented by the Butterworth-Van Dyke (BVD) model [13]. In the PR model, R, L, and C refer to the mechanical part of PRs, while C_P refers to the junction capacitor. Before the PR-based stage, there is a switched-capacitor pre-step-down stage, where switches S1-4 and flying capacitor C_1 switch between series and parallel modes. In the series mode, S1 and S3 are turned on, putting C_1 in series with the PR-based stage. In the parallel mode, S2 and S4 are turned on, putting C_1 in parallel with the PR-based stage. By this flying capacitor mechanism, C_1 is clamped to half the input voltage, lowering the voltage stress of the switches in the SC network and the equivalent input voltage to the PR-based stage.

The operation waveforms and modes are shown in Fig. 3 and Fig. 4. The converter operates over a sequence of 7 individual phases in a repeating manner with a period set by the SC circuit, with 2 of the 7 phases having alternating connection modes to ensure flying capacitor charge balancing. Across the 7 phases, there are 3 possible states the PR can be in: a connected PR state, a shorted PR state, and an opened PR state. As shown in Fig. 4, no switch connects the output of the PR in phases 1A and 1B, and thus in this opened PR state, the inductive PR current, $I_{L,PR}$, internally discharges junction capacitor, C_P, which charges V_{P2} until it reaches V_o to enable ZVS for S6. In phase 1A, the flying capacitor, C_1, is connected in the up (series) position, while in the next cycle in phase 1B, C_1, is connected in the down (parallel) position. In either case, once there is zero voltage across S6, it is turned on, connecting the PR to the output and beginning phases 2A and 2B, where the PR delivers energy from input to output while soft-charging flying capacitor C_1 via D (series operation) in 2A, or soft-discharging C_1 via $I_{L,PR}$ (parallel operation) in 2B, ensuring charge balance of C_1. Then, switches S1-4 are all opened in phase 3, open circuiting the PR, where $I_{L,PR}$ internally discharges C_P until $V_{P1} = V_o$ to enable ZVS for S5. Once $V_{P1} = V_o$, S5 is also turned on with S6, shorting the PR to ensure the continuity of the resonant current. This phase ends when $I_{L,PR}$ crosses zero and reserves its polarity.

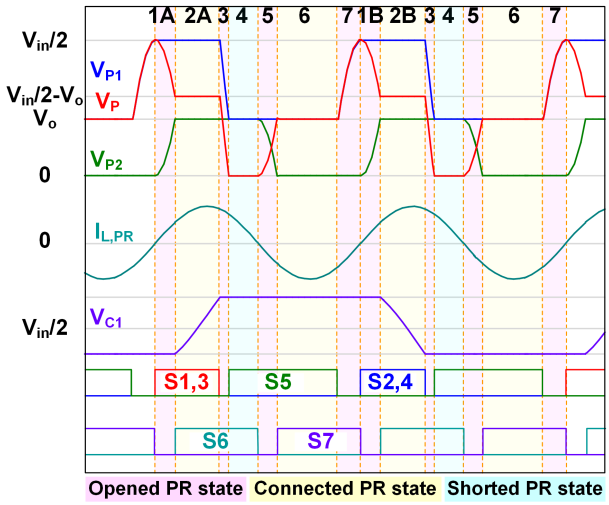

Fig. 3. Operation waveforms of series/parallel piezoelectric resonator converter

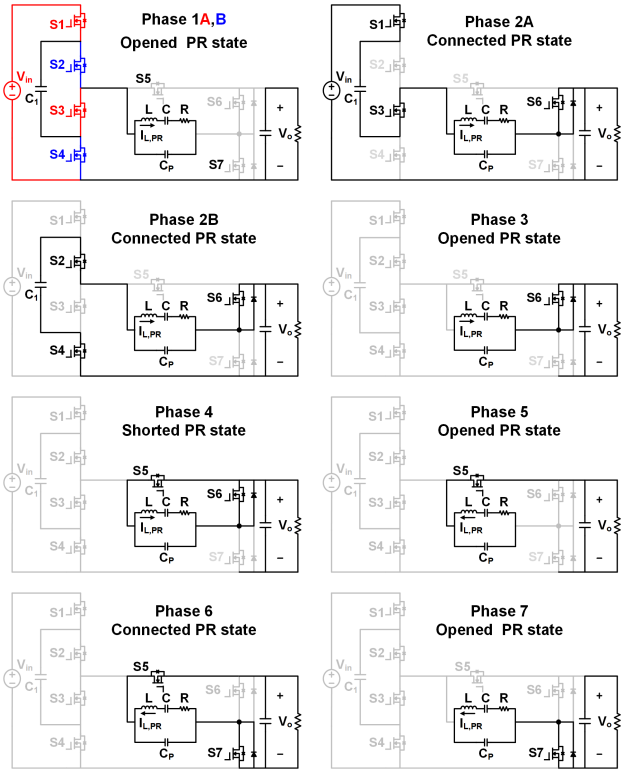

Fig. 4. Operation phases of series/parallel piezoelectric resonator converter

At this point, S6 is turned off, beginning phase 5, where the PR is now in the opened state, and $I_{L,PR}$ charges C_P, thereby discharging V_{P2} until it reaches zero to enable ZVS turn-on of S7. At this point, S7 turns on in phase 6, connecting the PR to the output via ground, thereby releasing stored energy to the load. Phase 7 begins when S5 turns off, opening the PR, where $I_{L,PR}$ charges CC_P until VP1 reaches V_{IN}, minimizing switching loss across S1,3/S2,4 in the next SC cycle.

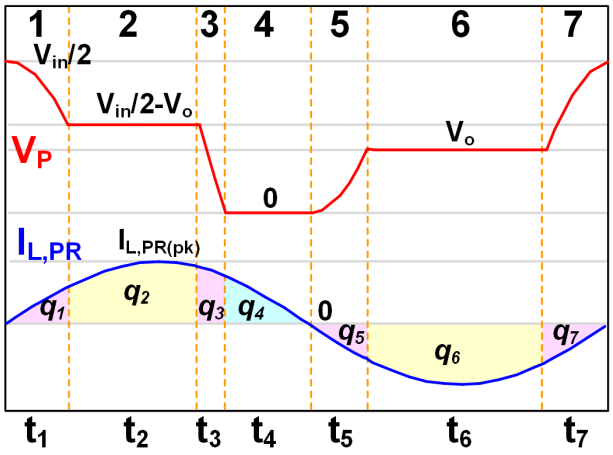

Fig. 5. Waveforms of a PR cycle

III. Steady-State Operation Analysis

To understand the piezoelectric resonator's behavior, operation, and performance in the proposed SPPR converter, the voltage conversion ratio (VCR), charge transfer, and amplitude of the resonant current will be mathematically derived and discussed. Finally, the loss due to the mechanical vibration of the PR can be found.

A. Voltage Conversion Ratio and PR Utilization

The steady-state waveforms over a PR cycle are shown in Fig. 5. In the steady-state operation over a cycle, a PR must follow the conservation of charge (CoC) and conservation of energy (CoE) to balance the charge and energy [3], [12]. Therefore, the CoC of C and C_P must hold in (1) and (2) where q_n is the charge in each phase.

$$q_1 + q_2 + q_3 + q_4 + q_5 + q_6 + q_7 = 0 \tag{1}$$

$$q_1 + q_3 + q_5 + q_7 = 0 \tag{2}$$

By substituting (2) into (1), it can be found that the charge transfer must be balanced in the connected and shorted states, which is expressed as:

$$q_2 + q_4 + q_6 = 0 \tag{3}$$

On the other hand, only the connected states, phase 2 and phase 6, transfer energy in the seven phases of the SPPR converter, and hence the CoE must hold:

$$E_2 + E_6 = V_2 q_2 + V_6 q_6 = (V_{in}/2 - V_o)\, q_2 + V_o q_6 = 0 \tag{4}$$

Then, inserting (3) into (4) using $q_6 = -(q_2 + q_4)$, the voltage conversion ratio of the SPPR converter can be found as:

$$0 \le \frac{V_o}{V_{in}} = \frac{1}{2}\frac{q_2}{2q_2 + q_4} \le \frac{1}{4} \tag{5}$$

It can be observed that the voltage conversion ratio depends on the ratio of the charge in the connected state, phase 2, and the shorted state, phase 4, within the positive cycle of $I_{L,PR}$. By assuming that the charge in opened states, phases 1 and 3, are small and negligible, the VCR reaches its maximum value, which equals 0.25, when the duration of phase 2 is the entire positive cycle of $I_{L,PR}$; on the other hand, the VCR reaches its minimum value, which equals 0, when the duration of phase 4 equals the entire positive cycle of $I_{L,PR}$ implying zero energy transfer. Compared to the baseline PR-based converter presented in [12], the voltage conversion ratio range is halved due to the pre-step-down SC network, which reduces the effective input voltage for the PR stage and leads to a more efficient operation of the PR at a higher step-down scenario.

The PR utilization factor, K, first introduced in [12], is a factor in evaluating how efficient the PR is in a specific implementation and phase sequence regardless of material, size, loss coefficients, etc. The PR utilization factor is defined by the idea of effective charge transferred, which is the portion of the charge in the connected and shorted states that are finally delivered to the output.

Here, the PR utilization factor of the SPPR converter can be defined as:

$$K = \frac{|q_2| + |q_6|}{|q_2| + |q_4| + |q_6|} \tag{6}$$

Substituting (3) and (4) into (6), the PR utilization factor can be rearranged into a form of V_{in} and V_o, which is shown in (7).

$$0.5 \le K = \frac{V_{in}}{2\,(V_{in} - 2V_o)} \le 1 \tag{7}$$

According to (7), K is 1 when the VCR equals 0.25, and K is 0 when VCR equals 0, implying that the PR is most efficient when the SPPR converter operates at the maximum conversion ratio where the duration of the resonant current circulating phase, phase 4, is minimum. That is to say that as VCR reduces, K reduces as well, showing an inefficient use of the PR, and resulting in overall efficiency reduction. Compared to the baseline PR-based converter in [12], (5) and (7) show that the optimal efficiency is shifted down from the conversion ratio of 0.5 to 0.25, which is more suitable for a higher step-down application.

B. Charge Transfer and PR Resonant Current under a Lossy Model

To derive the PR resonant current, $I_{L,PR}$, for mechanical loss, the total charger transferred and stored in the PR must be first addressed. There are two parts of charge transferred or stored in the PR: 1) Q_{out}, which are transferred to the output, and 2) Q_{ZVS}, that are used to soft charge/discharge C_P for ZVS turn-on. Therefore, the total charge can be expressed as:

$$Q_{total} = Q_{out} + Q_{ZVS} = \frac{I_o}{Kf} + C_P V_{in} \tag{8}$$

On the other hand, the total charge can also be expressed in terms of $I_{L,PR}$ as:

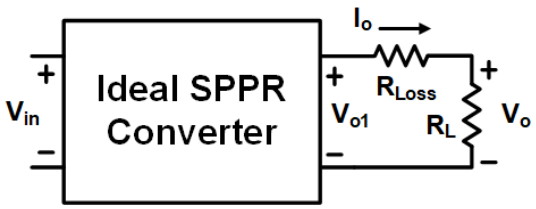

Fig. 6. Lossy model of the SPPR converter

$$Q_{total} = 2\int_0^{\frac{1}{2f}} i_{L,PR}(t)dt \tag{9}$$

Where,

$$i_{L,PR}(t) = I_{L,PR(pk)}\sin(\omega t)$$

By equating (8) and (9), the amplitude of the PR resonant current, $I_{L,PR(pk)}$, can be derived:

$$I_{L,PR(pk)} = \frac{\pi}{2}\left(\frac{I_o}{K} + fC_P V_{in}\right) \tag{10}$$

Here, the $I_{L,PR(pk)}$ is derived in the ideal (lossless) condition; however, sometimes, the losses inside the PR may make the $I_{L,PR(pk)}$ in (10) inaccurate in practice, where the calculation should be derived for V_{o1}/V_{in} conversion ratio instead of V_o/V_{in}, as shown in Fig. 6. Therefore, the $I_{L,PR(pk)}$ should be modified to include the amplitude difference caused by losses.

Due to the introduction of the lossy resistor, R_{Loss}, K in the lossy model can be expressed as:

$$K_{lossy} = \frac{V_{in}}{2(V_{in} - 2V_{o1})} = \frac{V_{in}}{2\left(V_{in} - 2\left(1 + \frac{R_{Loss}}{R_L}\right)V_o\right)} \tag{11}$$

Then, (11) can be inserted to (10) to get the $I_{L,PR(pk)}$ with the losses effect where R_{Loss} can be found in (12), which is derived by equating the losses in the PR and losses in the Thevenin equivalent loss resistance, as $I_{LPR,(pk)}^2 R = I_o R_{Loss}$. $V_{in,PR}$ in (12) is the effective input voltage of the PR stage, which is $V_{in}/2$ in the proposed SPPR converter.

$$R_{Loss} = \frac{-b \pm \sqrt{b^2 - 4ac}}{2a} \tag{12}$$

where,

$$a = \left(\frac{\pi P_o}{V_{in,PR}R_L}\right)^2, c = \pi^2\left(fC_P V_{in,PR} + I_o - \frac{P_o}{V_{in,PR}}\right)^2$$

$$b = -\frac{2}{R_L}\left[\pi^2\left(fC_P V_{in,PR} + I_o - \frac{P_o}{V_{in,PR}}\right)\frac{P_o}{V_{in,PR}} + I_o^2\frac{R_L}{R}\right]$$

Fig. 7 shows the comparison of the lossy and lossless models along with simulation results under a 48/10 SPPR converter at 5W output with a PR mechanical resistor of 2.4Ω, which is obtained from [12]. In the figure, the lossless model overestimates the resonant current, while the proposed lossy model accurately predicts the behavior of the PR converter. With the lossy model, the efficiency can be more accurately

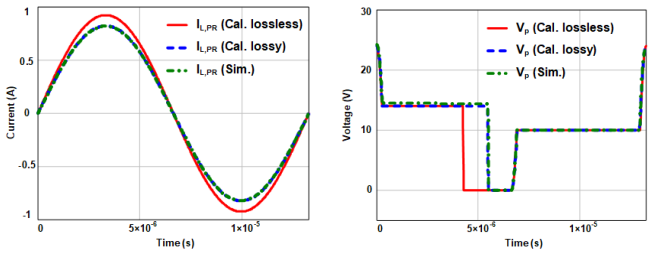

(a) PR resonant current in a cycle (b) PR voltage in a cycle

Fig. 7. Lossy and lossless model comparison

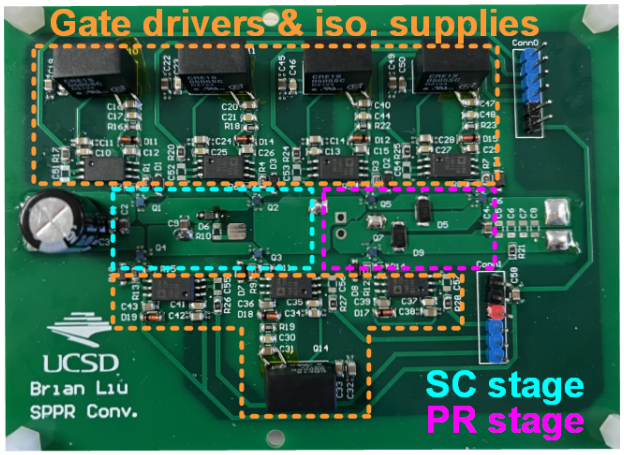

(a) Top view

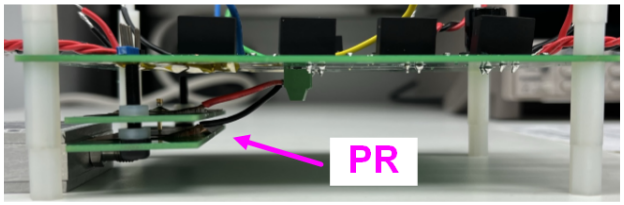

(b) Side view

Fig. 8. Prototype of series/parallel piezoelectric resonator converter

estimated, and the achievable operation range can be better predicted, providing better insights while designing the PR-based converter and selecting PRs.

Finally, with $I_{L,PR(pk)}$ calculated from (10)-(12), the loss of the PR can be written as:

$$P_{loss,PR} = \frac{1}{2}I_{L,PR(pk)}^2 R \tag{13}$$

IV. Implementations and Experiment Results

The proposed series/parallel piezoelectric resonator converter prototype is built alongside a baseline PR-only converter (which shares the same components and PCB design) with a commercially available PZT-based PR as shown in Fig. 11. The prototype can be operated in SPPR mode or baseline PR mode by different driving signals, enabling a fair performance comparison. The experimental components and parameters are shown in Table I. In the implementation, the disk-shaped

TABLE I
EXPERIMENTAL PARTS AND PARAMETERS

Parts/Parameters	Values	implementation
Switches (S1-S7)	80V, 10A, 20mΩ	EPC2214
Piezoelectric resonator	20/0.2 mm	PIC181
S6,7 parallel diode	40V, 2A	PMEG4020EP
Gate driver	Isolated, 2.3A	ADUM4120
Digital controller	150 MHz	TMS320F28335
Input voltage range V_{in}	48 V	-
Output voltage range V_o	5-10 V	-
Output current range I_o	0.05-0.3 A	-
flying capacitor C_1	4.7 μF	MLCC (0805)
Resonant frequency f_r	$\approx$ 113 kHz	Piezo resonator
Anti-resonant frequency f_{ar}	$\approx$ 129 kHz	Piezo resonator
Junction capacitor C_P	13.96 nF	Piezo resonator
Dielectric resistor R_P	11.73 kΩ	Piezo resonator
Mechanical capacitor C	4.2 nF	Piezo resonator
Mechanical Inductor L	468.78 μH	Piezo resonator
Mechanical resistor R	0.48 Ω	Piezo resonator

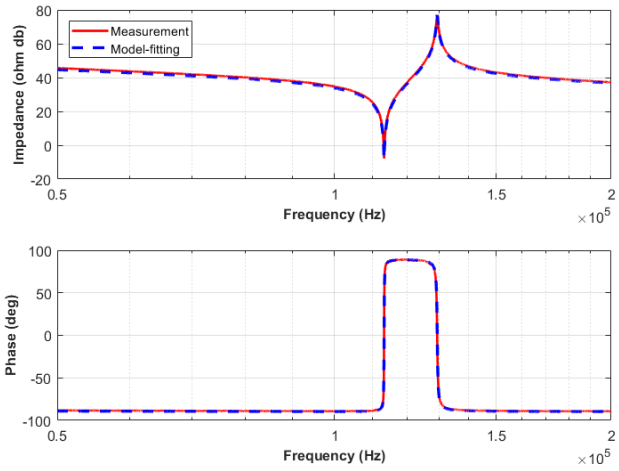

Fig. 9. The piezoelectric resonator(20/0.2mm PIC181) model-fitting results

piezoelectric resonator employed is made of PIC181 material operating in radial vibration mode with a size of (20/0.2)mm in diameter and thickness. The BVD model fitting result of disk-shaped PR is shown in Fig. 9. GaNFETs are utilized in the prototype for their excellent switching characteristics, minimizing switching losses in S1-4. The prototype is controlled by a DSP controller with open-loop control, where the synchronous rectifiers, S6 and S7, and the value of frequency, duty cycle, and deadtime are manually tuned to the desired operating point.

The steady-state operation waveform at a 48/10V conversion ratio for both the SPPR and PR converters are shown in Fig. 10(a) and 10(b). As can be seen in Fig. 10(a), the flying capacitor is soft-charged/discharged, and S5-S7 achieve ZVS as desired. It can be observed that the duration of the input-output connected phase, phase 2, is much longer in the SPPR converter, implying better PR utilization and hence better efficiency.

The efficiency comparison of the SPPR and PR converter at the same input/output voltage is shown in Fig. 11(a). As can be seen from the measurement results, the SPPR converter achieves a peak efficiency of 95.27%, which is up to a 14.17% improvement over the baseline PR converter, since the

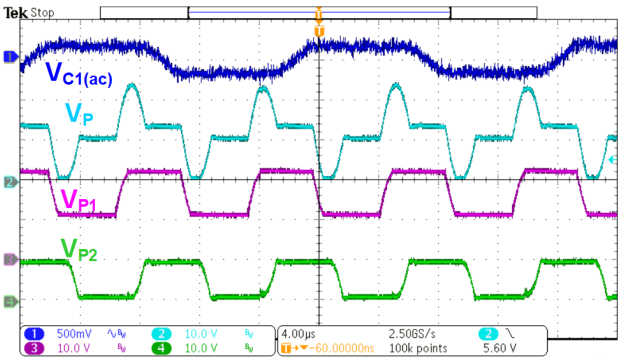

(a) SPPR waveforms@ 48/10V, 2W

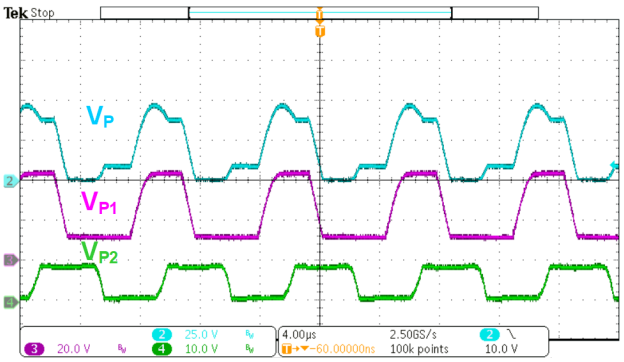

(b) PR waveforms@ 48/10V, 2W

Fig. 10. Steady-state waveforms

equivalent VCR of the SPPR is much higher than the baseline PR converter, whose VCR are 0.42 for the SPPR converter and 0.21 for the baseline PR converter. The calculated efficiency for the SPPR converter is pretty close to the measurement results. The model for the baseline PR converter, however, diverges significantly in the measurement results, which prior literature has also observed at larger step-down ratios and higher power [3], [14]. While spurious mode excitation is a plausible hypothesis, there is not currently an accurate model to predict this behavior; this will be the subject of future work.

Fig. 11(b) shows the frequency variation comparison of the baseline PR-based and SPPR converters at different output currents. It can be observed that the operating frequency decreases with the increase of output current/power due to the shorter opened states and longer connected and shorted states in both the baseline PR-based and SPPR converter. Moreover, at a given output current, the one with a higher VCR value is operated at a lower frequency.

Fig. 12 shows the efficiencies of the SPPR converter at the 48V input voltage with different output voltages and currents. It can be seen that the SPPR converter outperforms the baseline PR converter at all operation points. The efficiency curves also show that, at a given output current, the efficiency decreases with the decrease in conversion ratio, which matches the analysis in Section III.

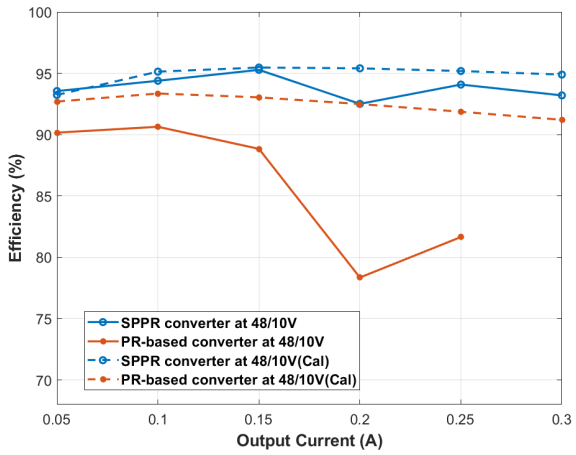

(a) Efficiency comparison of the SPPR and PR-based converter at 48/10V

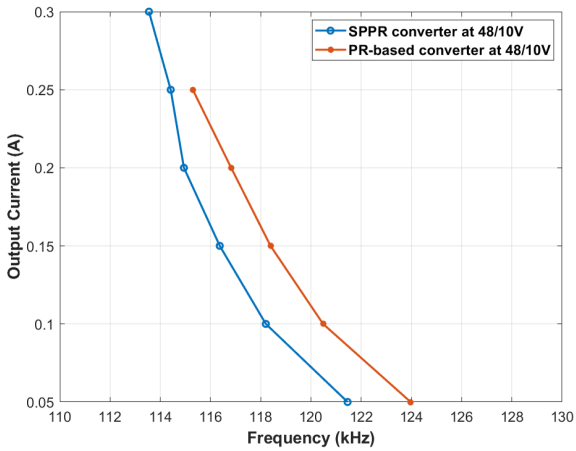

(b) Frequency variation of the SPPR and PR-based converter at 48/10V

Fig. 11. Efficiency and frequency variation comparison of SPPR and PR-based converter at 48V/10V

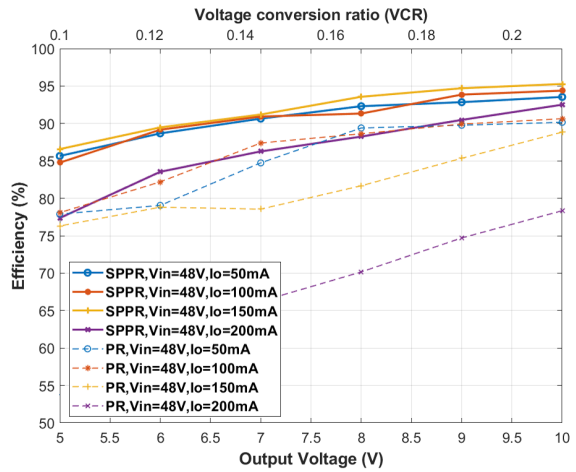

Fig. 12. Efficiency comparison of SPPR and PR-based converter at $48V_{in}$

V. Conclusion

This work proposed a SPPR converter to improve the performance of a baseline PR converter when a larger than 2:1 conversion ratio is required. The behavior of the SPPR converter was mathematically analyzed and verified by simulations. A physical prototype of the proposed SPPR converter alongside the baseline PR converter with a 20/0.2mm disk-shaped PIC181 PR was built to demonstrate the concept of the SPPR converter. Measurement results demonstrated a 95.27% peak efficiency, and up to a 14.17% efficiency improvement compared to the baseline PR converter at a 48/10V conversion ratio.

References

[1] G.-S. Seo, J.-W. Shin, and B.-H. Cho, "A magnetic component-less series resonant converter using a piezoelectric transducer for low profile application," in *The 2010 International Power Electronics Conference - ECCE ASIA -*, 2010, pp. 2810–2814.

[2] J. D. Boles, E. Ng, J. H. Lang, and D. J. Perreault, "Dc-dc converter implementations based on piezoelectric transformers," *IEEE Journal of Emerging and Selected Topics in Power Electronics*, pp. 1–1, 2021.

[3] B. Pollet, G. Despesse, and F. Costa, "A new non-isolated low-power inductorless piezoelectric dc-dc converter," *IEEE Transactions on Power Electronics*, vol. 34, no. 11, pp. 11 002–11 013, 2019.

[4] B. Pollet, F. Costa, and G. Despesse, "A new inductorless dc-dc piezoelectric flyback converter," in *2018 IEEE International Conference on Industrial Technology (ICIT)*, 2018, pp. 585–590.

[5] B. Pollet, G. Despesse, and F. Costa, "A new non-isolated low-power inductorless piezoelectric dc-dc converter," *IEEE Transactions on Power Electronics*, vol. 34, no. 11, pp. 11 002–11 013, 2019.

[6] E. L. Horsley, A. V. Carazo, N. Nguyen-Quang, M. P. Foster, and D. A. Stone, "Analysis of inductorless zero-voltage-switching piezoelectric transformer-based converters," *IEEE Transactions on Power Electronics*, vol. 27, no. 5, pp. 2471–2483, 2012.

[7] C. Lin and F. Lee, "Design of a piezoelectric transformer converter and its matching networks," in *Proceedings of 1994 Power Electronics Specialist Conference - PESC'94*, vol. 1, 1994, pp. 607–612 vol.1.

[8] C. R. Sullivan, B. A. Reese, A. L. F. Stein, and P. A. Kyaw, "On size and magnetics: Why small efficient power inductors are rare," in *2016 International Symposium on 3D Power Electronics Integration and Manufacturing (3D-PEIM)*, 2016, pp. 1–23.

[9] J. D. Boles, P. L. Acosta, Y. K. Ramadass, J. H. Lang, and D. J. Perreault, "Evaluating piezoelectric materials for power conversion," in *2020 IEEE 21st Workshop on Control and Modeling for Power Electronics (COMPEL)*, 2020, pp. 1–8.

[10] M. Touhami, G. Despesse, and F. Costa, "A new topology of dc-dc converter based on piezoelectric resonator," *IEEE Transactions on Power Electronics*, vol. 37, no. 6, pp. 6986–7000, 2022.

[11] W. D. Braun, Z. Tong, and J. Rivas-Davila, "Inductorless soft switching dc-dc converter with an optimized piezoelectric resonator," in *2020 IEEE Applied Power Electronics Conference and Exposition (APEC)*, 2020, pp. 2272–2278.

[12] J. D. Boles, J. J. Piel, and D. J. Perreault, "Enumeration and analysis of dc-dc converter implementations based on piezoelectric resonators," *IEEE Transactions on Power Electronics*, vol. 36, no. 1, pp. 129–145, 2021.

[13] K. Van Dyke, "The piezo-electric resonator and its equivalent network," *Proceedings of the Institute of Radio Engineers*, vol. 16, no. 6, pp. 742–764, 1928.

[14] B. Pollet, M. Touhami, G. Despesse, and F. Costa, "Effects of disc-shaped piezoelectric size reduction on resonant inductorless dc-dc converter," in *2019 20th International Conference on Solid-State Sensors, Actuators and Microsystems & Eurosensors XXXIII (TRANSDUCERS & EUROSENSORS XXXIII)*, 2019, pp. 1423–1426.